Exploring the 3-(phenylethynyl)-9H-carbazole unit in the search of deep-blue emitting fluorophores

Roger Bujaldón [a], Nikola Peřinka [b], Marta Reig [a], Alba Cuadrado [a], Clara Fabregat [a], Mercè Font-Bardía [c], Eugenia Martínez-Ferrero[b,**], Dolores Velasco a [3*]

[a] Grup de Materials Orgànics, Institut de Nanociència i Nanotecnologia (IN2UB), Departament de Química Inorgànica i Orgànica (Secció de Química Orgànica), Universitat de Barcelona, Martí i Franquès 1, E-08028, Barcelona, Spain

[b] Eurecat, Centre Tecnològic de Catalunya, Printed Electronics & Embedded Devices Unit, E-08302, Mataró, Spain

[c] Unitat de Difracció de Raigs-X, Centres Científics i Tecnològics (CCiT), Universitat de Barcelona, Solé i Sabaris 1-3, E-08028, Barcelona, Spain

[*] Corresponding Author:

E-mail addresses: eugenia.martinez@eurecat.org (E. Martínez-Ferrero), dvelasco@ub.edu (D. Velasco).

Abstract

Two new types of molecular constructions based on the 3-(phenylethynyl)-9H-carbazole moiety have been developed. Specifically, the synthesized bicarbazole and triethynylbenzene derived fluorophores display emission ranging from deep-blue to green-blue in the solid state, depending on the N-alkyl chain length and their intermolecular arrangement, which has been elucidated from the crystallographic data. Their photophysical and electrochemical properties have permitted the construction of blue OLEDs with a simple device architecture compatible with the solution-processing. In addition, the combination of the synthesized emitters with a small ratio of commercial iridium complexes has allowed the preparation of pure white OLEDs by spin coating the different layers. The characteristics of the emitted white light depend not only on the emissive layer composition but also on the applied voltage, standing as two key factors to easily modulate the color temperature.

Keywords:

Carbazole
Organic materials
Deep-blue emitters
Luminescence
Color temperature
WOLEDs

1. Introduction

Organic Light-Emitting Diodes (OLEDs) have attracted a lot of attention in the past two decades due to their many potential benefits in comparison with the current available lighting technologies, such as low weight, flexibility, large area compatibility, high luminance even at low observation angles and high light conversion efficiency [1,2]. However, the high production cost attached to low throughput and expensive fabrication techniques and the limited availability of improved fluorophores remain as the main obstacles for their introduction in the market. Concerning this, the introduction of the solution processing strategy represents an alternative for the low-cost manufacture of flat displays and lighting [3–6]. Devices based on small molecules have shown very high performances when integrated into evaporation-made devices, so the research of new emitters suitable for the solution processing is a topic of interest within the scientific community [7–10]. Another important point to consider in full operational OLEDs viability is the need of enhanced blue emitters, necessary in both full-color displays and WOLEDs (White Light-Emitting Diodes) [11–13]. Since the latter technology is still advancing, it requires further investigation to potentially pave the way for low-cost fabrication of WOLEDs.

The structural design of the blue emitter is crucial to adapt and modulate the color emission and improve the device performance. Carbazole-based molecules are known to provide noteworthy features, such as good hole transport and strong emission that can be modified synthetically, and thus find numerous applications in the optoelectronic field [14–20]. Additionally, the carbazole core acts as a relatively weak π-donor moiety, which is of interest to the research on deep blue dyes (Commission Internationale de l'Eclairage y coordinate value up to 0.1) [21–24]. Synthetically, the structures of the herein presented carbazole derivatives consist in the attachment of additional aromatic moieties to the carbazole core through a triple bond spacer. This spacer provides rigidity and planarity, favoring conjugation and π-electron delocalization, which is of interest in the design of new fluorophores [25–27]. In fact, the 3-(phenylethynyl)-9H-carbazole unit as a synthetic building block has already proved to efficiently provide blue emission in OLEDs, especially within the deep-blue region [28,29]. With this in mind, two new molecular constructions have been considered, namely 6,6′ -bis (phenylethynyl)-9H,9′H-3,3′ -bicarbazole and 1,3,5-tris((9H-carbazol-3-yl)ethynyl)benzene. In the former structure, two 3-(phenylethynyl)-9H-carbazole units are bonded through positions 3 and 3′ of the carbazole heterocycles, whereas three carbazole moieties are attached to a central benzene ring in the latter (shown in Fig. 1). Also, the attachment of N-alkyl chains of different lengths has been considered, since it can be a determining factor in conferring an adequate intermolecular disposition and more solubility in the conventional organic solvents required for the solution processing.

This study presents the development and characterization of new blue-emitting soluble compounds and their integration in OLED devices. Specifically, these compounds have been tested as blue emitters in nondoped OLEDs and in combination with soluble iridium complexes in WOLEDs (Fig. 1), resulting in a bulk heterojunction emissive layer with tunable white emission.

2. EXPERIMENTAL

2.1. Materials

All chemicals were of commercial grade and used as received. All solvents were dried and degassed by standard methods. Tetrahydrofuran (THF) was distilled from sodium/benzophenone and dichloromethane from CaH2. Anhydrous CHCl3 was purchased from Sigma-Aldrich and stored under nitrogen atmosphere. Flash chromatography was carried out over silica gel (Sigma-Aldrich, 230–400 mesh).

2.2. Synthesis and characterization

2.2.1. Synthesis of 9,9′ -diethyl-9H,9′H-3,3′ -bicarbazole (1a)

9-Ethyl-9H-carbazole (5.1 g, 26 mmol) was dissolved in anhydrous CHCl3 (40 mL) under inert atmosphere. Next, anhydrous FeCl3 (16.1 g, 102 mmol) was added, and the reaction mixture was stirred at room temperature for 30 min. After, the mixture was diluted with methanol (100 mL) and the solvent was distilled off under reduced pressure. The mixture was purified by flash column chromatography using a mixture of hexane and CH2Cl2 (10:1 v/v) as eluent. Compound 1a was obtained in a yield of 89% (4.4 g, 11 mmol). 1H NMR (400 MHz, CDCl3) δ (ppm): 8.42 (d, J = 1.8 Hz, 2H), 8.20 (d, J = 7.8 Hz, 2H), 7.84 (dd, J = 8.4 Hz, J = 1.8 Hz, 2H), 7.51 (d, J = 8.4 Hz, 2H), 7.48 (ddd, J = 8.1 Hz, J = 7.5 Hz, J = 1.2 Hz, 2H), 7.44 (d, J = 7.5 Hz, 2H), 7.26 (dd, J = 8.1 Hz, J = 7.8 Hz, J = 1.2 Hz, 2H), 4.43 (q, J = 7.9 Hz, 4H), 1.49 (t, J = 7.9 Hz, 6H).

2.2.2. Synthesis of 9,9′ -dihexyl-9H,9′H-3,3′ -bicarbazole (1b)

*Follow*ing the synthetic procedure described for compound 1a, 9-hexyl-9H-carbazole (5.1 g, 20 mmol) was dissolved in anhydrous CHCl3 (38 mL) and then, anhydrous FeCl3 (13 g, 80 mmol) was added. The mixture was purified by flash column chromatography using a mixture of hexane and CH2Cl2 (10:1 v/v) as eluent. Compound 1b was obtained in a yield of 58% (2.9 g, 5.8 mmol). 1H NMR (400 MHz, CDCl3) δ (ppm): 8.42 (d, J = 1.7 Hz, 2H), 8.20 (d, J = 7.8 Hz, 2H), 7.84 (dd, J = 8.5 Hz, J = 1.7 Hz, 2H), 7.52–7.43 (m, 6H), 7.26 (ddd, J = 7.8 Hz, J = 7.0 Hz, J = 1.0 Hz, 2H), 4.35 (t, J = 7.2 Hz, 4H), 1.97–1.88 (m, 4H), 1.49–1.27 (m, 12H), 0.89 (t, J = 7.2 Hz, 6H).

2.2.3. Synthesis of 9,9′ -diethyl-6,6′ -diiodo-9H,9′H-3,3′ -bicarbazole (2a)

9,9′ -Diethyl-9H,9′H-3,3′ -bicarbazole 1a (1.6 g, 4.1 mmol) was dissolved in glacial acetic acid (60 mL) under reflux. Then, KI (0.91 g, 5.5 mmol) was added, and the mixture was stirred under reflux for 10 min. Afterwards, KIO3 (1.3 g, 6.1 mmol) was added and the mixture was stirred at reflux for 40 min. The crude was cooled down to room temperature and filtered. The solid was washed with NaHCO3 (sat.), extracted with CH2Cl2 and dried over anhydrous Na2SO4. After filtering, the solvent was distilled off under reduced pressure and purified by flash column chromatography using a mixture of hexane and ethyl acetate (20:1 v/v) as eluent. Compound 2a was obtained in a yield of 33% (0.87 g, 1.4 mmol). 1H NMR (400 MHz, CDCl3) δ (ppm): 8.50 (d, J = 1.6 Hz, 2H), 8.34 (d, J = 1.6 Hz, 2H), 7.84 (dd, J = 8.6 Hz, J = 1.6 Hz, 2H), 7.73 (dd, J = 8.5 Hz, J = 1.6 Hz, 2H), 7.50 (d, J = 8.6 Hz, 2H), 7.23 (d, J = 8.5 Hz, 2H), 4.39 (q, J = 7.4 Hz, 4H), 1.25 (t, J = 7.4 Hz, 6H).

2.2.4. Synthesis of 9,9′ -dihexyl-6,6′ -diiodo-9H,9′H-3,3′ -bicarbazole (2b)

Similarly to the synthetic procedure described for 2a, 9,9′ -dihexyl- 9H,9′H-3,3′ -bicarbazole 1b (1.5 g, 3.1 mmol) was dissolved in glacial acetic acid (50 mL) and KI (0.69 g, 4.1 mmol) and KIO3 (0.98 g, 4.6 mmol) were subsequently added. After stirring at reflux for 15 min, the solution was neutralized with NaHCO3 and extracted with CH2Cl2. The crude was purified by flash column chromatography using a mixture of hexane and CH2Cl2 (20:1 v/v) as eluent.

Compound 2b was obtained in a yield of 36% (0.83 g, 1.1 mmol). 1H NMR (400 MHz, CDCl3) δ (ppm): 8.49 (d, J = 1.6 Hz, 2H), 8.33 (d, J = 1.6 Hz, 2H), 7.82 (dd, J = 8.8 Hz, J = 1.6 Hz, 2H), 7.72 (dd, J = 8.8 Hz, J = 1.6 Hz, 2H), 7.48 (d, J = 8.8 Hz, 2H), 7.21 (d, J = 8.8 Hz, 2H), 4.31 (t, J = 7.3 Hz, 4H), 1.90–1.87 (m, 4H), 1.40–1.25 (m, 12H), 0.88 (t, J = 7.0 Hz, 6H).

2.2.5. Synthesis of 9,9′ -diethyl-6,6′ -bis(phenylethynyl)-9H,9′ H-3,3′ - bicarbazole (3a)

9,9′ -Diethyl-6,6′ -diiodo-9H,9′H-3,3′ -bicarbazole 2a (0.46 g, 0.72 mmol), CuI (12 mg, 0.063 mmol) and Pd(PPh3)2Cl2 (21 mg, 0.018 mmol) were placed in a round-bottomed flask. Then, the system was evacuated in vacuo and filled up with nitrogen thrice. Afterwards, triethylamine (0.24 mL, 1.7 mmol), phenylacetylene (0.19 mL, 1.7 mmol) and anhydrous THF (20 mL) were added. The reaction mixture was stirred at room temperature for 24 h. After that, the solvent was distilled off under reduced pressure and the crude was purified by flash column chromatography using a mixture of hexane and ethyl acetate (20:1 v/v) as eluent. Compound 3a was obtained in a yield of 47% (0.20 g, 0.33 mmol). 1H NMR (400 MHz, CDCl3) δ (ppm): 8.42 (d, J = 1.4 Hz, 2H), 8.41 (d, J = 1.1 Hz, 2H), 7.86 (dd, J = 8.5 Hz, J = 1.7 Hz, 2H), 7.67 (dd, J = 8.3 Hz, J = 1.4 Hz, 2H), 7.61 (dd, J = 8.3 Hz, J = 1.6 Hz, 4H), 7.52 (d, J = 8.3 Hz, 2H), 7.41 (d, J = 8.4 Hz, 2H), 7.36–7.32 (m, 6H), 4.43 (q, J = 7.5 Hz, 4H), 1.51 (t, J = 7.2 Hz, 6H). 13C NMR (100 MHz, CDCl3) δ (ppm): 140.2, 139.6, 133.8, 131.6, 129.5, 128.5, 127.9, 126.1, 124.4, 124.1, 123.3, 123.1, 119.3, 113.5, 109.3, 108.8, 91.3, 87.7, 38.1, 14.7. HRMS (ESI-MS) (m/z): calcd for C44H33N2 (M + H)+, 589.2638; found 589.2637.

2.2.6. Synthesis of 9,9′ -dihexyl-6,6′ -bis(phenylethynyl)-9H,9′H-3,3′ - bicarbazole (3b)

Following the synthetic procedure described for compound 3a, 9,9′ -dihexyl-6,6′ -diiodo-9H,9′H-3,3′ -bicarbazole 2b (0.31 g, 0.41 mmol), CuI (8 mg, 0.04 mmol), Pd(PPh3)2Cl2 (14 mg, 0.020 mmol), trimethylamine (0.17 mL, 1.2 mmol), phenylacetylene (0.13, 1.2 mmol) and anhydrous THF (18 mL) were stirred at room temperature for 24 h. The crude was purified by flash column chromatography using a mixture of hexane and CH2Cl2 (5:1 v/v) as eluent. Compound 3b was obtained in a yield of 57% (0.165 g, 0.24 mmol). 1H NMR (400 MHz, CDCl3) δ (ppm): 8.42 (d, J = 1.6 Hz, 2H), 8.41 (d, J = 1.4 Hz, 2H), 7.85 (dd, J = 8.5 Hz, J = 1.6 Hz, 2H), 7.67 (dd, J = 8.4 Hz, J = 1.4 Hz, 2H), 7.60 (dd, J = 8.3 Hz, J = 1.6 Hz, 4H), 7.51 (d, J = 8.5 Hz, 2H), 7.39 (d, J = 8.4 Hz, 2H), 7.37–7.33 (m, 6H), 4.32 (t, J = 7.2 Hz, 4H), 1.95–1.87 (m, 4H), 1.44–1.37 (m, 4H), 1.36–1.28 (m, 8H), 0.87 (t, J = 7.0 Hz, 6H). 13C NMR (100 MHz, CDCl3) δ (ppm): 140.6, 139.9, 133.6, 131.5, 129.3, 128.3, 127.7, 125.9, 124.2, 124.0, 123.1, 123.1, 119.0, 113.2, 109.3, 108.8, 90.9, 87.6, 43.3, 31.6, 29.0, 27.0, 22.6, 14.0. HRMS (ESI-MS) (m/z): calcd for C52H49N2 (M + H)+, 701.3890; found 701.3897.

2.2.7. Synthesis of 1,3,5-tris((9-ethyl-9H-carbazol-3-yl)ethynyl)benzene (4a)

9-ethyl-3-iodo-9H-carbazole (920 mg, 2.85 mmol), Pd(PPh3)2Cl2 (210 mg, 0.24 mmol) and CuI (91 mg, 0.48 mmol) and triethynylbenzene (300 mg, 2.0 mmol) were dissolved in anhydrous THF (40 mL) under inert atmosphere. Afterwards, triethylamine (1 mL, 7.2 mmol) was added and the reaction mixture was stirred at room temperature overnight. Then, the solvent was distilled off under reduced pressure and the crude was purified by flash column chromatography using a mixture of hexane and CH2Cl2 (3:1 v/v) as eluent. Compound 4a was obtained in a yield of 13% (87 mg, 0.12 mmol). 1H NMR (400 MHz, CDCl3) δ (ppm): 8.34 (d, J = 1.3 Hz, 3H), 8.13 (d, J = 7.8 Hz, 3H), 7.73 (s, 3H), 7.67 (dd, J = 8.4 Hz, J = 1.3 Hz, 3H), 7.51 (ddd, J = 8.1 Hz, J = 7.3 Hz, J = 1.1 Hz, 3H), 7.44 (d, J = 8.1 Hz, 3H), 7.41 (d, J = 8.4 Hz, 3H), 7.26 (dd, J = 7.8 Hz, J = 7.3 Hz, 3H), 4.40 (q, J = 7.7 Hz, 6H), 1.47 (t, J = 7.7 Hz, 9H). 13C NMR (100 MHz, CDCl3) δ (ppm): 140.5, 139.9, 133.5, 129.5, 126.3, 124.7, 124.4, 123.2, 122.7, 120.8, 119.6, 113.1, 108.7, 108.7, 92.0, 86.6, 37.9, 14.0. HRMS (ESI-MS) (m/z): calcd for C54H40N3 (M + H)+, 730.3217; found 730.3213.

2.2.8. Synthesis of 1,3,5-tris((9-(2-ethylhexyl)-9H-carbazol-3-yl)ethynyl) benzene (4b)

Following the synthetic procedure described for compound 4a, 9-(2-ethylhexyl)-3-iodo-9H-carbazole (1.3 g, 3.11 mmol), Pd(PPh3)2Cl2 (222 mg, 0.31 mmol) and CuI (103 mg, 0.51 mmol) were dissolved in anhydrous THF (40 mL), followed by the addition of triethylamine (1.4 mL, 10.1 mmol) and triethynylbenzene (326 mg, 2.2 mmol). After purification by flash column chromatography using hexane and CH2Cl2 (5:1 v/v), compound 4b was obtained in a yield of 10% (100 mg, 0.10 mmol). 1H NMR (400 MHz, CDCl3) δ (ppm): 8.33 (d, J = 1.2 Hz, 3H), 8.12 (d, J = 7.4 Hz, 3H), 7.73 (s, 3H), 7.65 (dd, J = 8.4 Hz, J = 1.2 Hz, 3H), 7.49 (dd, J = 8.4 Hz, J = 8.1 Hz, 3H), 7.41 (d, J = 8.4 Hz, 3H), 7.37 (d, J = 8.4 Hz, 3H), 7.26 (dd, J = 7.4 Hz, J = 8.1 Hz, 3H) 4.19 (d, J = 7.1 Hz, 6H), 2.20–2.05 (m, 3H), 1.43–1.21 (m, 24H), 0.93 (t, J = 7.2 Hz, 9H), 0.87 (t, J = 7.2 Hz, 9H). 13C NMR (100 MHz, CDCl3) δ (ppm): 141.5, 140.9, 133.5, 129.5, 126.2, 124.7, 124.3, 123.0, 122.6, 120.7, 119.5, 113.0, 109.4, 109.2, 92.0, 86.6, 47.7, 39.6, 31.2, 29.0, 24.6, 23.2, 14.2, 11.1. HRMS (ESI-MS): calcd for C72H76N3 (M + H)+, 982.6034; found
982.6043.

2.3. Instrumentation and methods

1H NMR (400 MHz) and 13C NMR (100 MHz) spectra were collected in a Varian Mercury spectrophotometer. NMR spectra have been processed with the MestRec Nova software. HRMS was performed in a LC/MSD-TOF Agilent Technologies apparatus by means of the electrospray (ESI-MS) technique. Single-crystal analyses were performed on a D8 Venture System equipped with a multilayer monochromator and a Mo microfocus (λ = 0.71073 Å). The frames were integrated with the Bruker SAINT software package using a narrow-frame algorithm. The structure was solved and refined using the Bruker SHELXTL Software Package. Thermogravimetric analyses (TGA) were performed in a TA Instruments Q50 at a heating rate of 20 ◦C min^{-1} under nitrogen atmosphere. Differential scanning calorimetry (DSC) thermograms were recorded in a TA Instruments Q2000 calorimeter at a scan rate of 10 ◦C min^{-1} under nitrogen atmosphere. Absorption spectra were registered in a Varian Cary UV–Vis–NIR 500E spectrophotometer. Emission spectra in solution (THF, 10 μM) were recorded in a PTI fluorimeter after excitation at λex = λabs,max. Photophysical measurements in the solid state were done on films deposited from a 1 mM dichloromethane solution by spin coating at 1500 rpm for 20 s and at 3500 rpm for 10 s followed by 5 min of thermal annealing at 50 ◦C. Fluorescence quantum yields in solution were determined using 1,4-bis(5-phenyl-2-oxazolyl)benzene (POPOP) as the standard (λex = 300 nm, Φ = 0.93 in cyclohexane) following a literature protocol [30]. Fluorescence quantum yields of thin films were determined by means of an integrating sphere.

Cyclic voltammograms were recorded in a microcomputercontrolled potentiostat/galvanostat Autolab with PGSTAT30 equipment and GPES software. A cylindrical three-electrode cell was used. The reference electrode was an Ag/Ag+ electrode (1 mM AgNO3 in acetonitrile). The counter and working electrodes were a platinum wire and a glassy-carbon electrode, respectively. All voltammetric curves were recorded under quiescent conditions, at a scan rate of 100 mV s^{-1} and under argon atmosphere. All solutions were prepared in dichloromethane (1 mM). Tetrabutylammonium hexafluorophosphate (TBAP) was used as the supporting electrolyte (0.1 M). All potentials were referred to the Fc+/Fc redox couple. The ionization potential values (IP) were estimated from the onset of the first oxidation peak as IP = oxEonset + 5.39, where 5.39 eV corresponds to the formal potential of the Fc+/Fc couple in the Fermi scale [31]. The electron affinity values (EA) were calculated as EA = IP - Egap. The optical gap energy values (Egap) were estimated from λonset of the absorption spectra.

Charge drift mobility measurements were performed by means of the TOF and XTOF methods. In the case of TOF, the organic compound was drop casted on pre-cleaned indium tin oxide (ITO) coated glass substrates followed by deposition of 80 nm of aluminium by thermal

vacuum evaporation (106 mbar) using a mask (area = 0.06 cm2). Photogeneration of charge carriers was carried out by light pulse through the ITO. A Keithley 6517B electrometer was used to apply external voltages with a pulsed third-harmonic Nd:YAG laser EKSPLA NL300 working (pulse duration of 3–6 ns, λ = 355 nm). A digital storage oscilloscope Tektronix TDS 3032C was used to record the TOF transients. For the XTOF technique, the aluminium was deposited on a glass substrate followed by the spin casting of the organic material. Electric field inside the layer was created by charging of a corona. Illumination with pulses of N2 laser (pulse duration of 2 ns, λ = 337 nm) generated charge carriers at the layer surface. The transient time (tt) was determined by the kink on the curve of the transient in the log - log scale. The drift mobility was calculated by the formula μ = d2/Utt, where d is the layer thickness and U is the surface potential at the moment of illumination. The field dependence of the hole mobility was determined according to the formula logμ = αE1/2.

2.4. OLED device fabrication and measurements

The glass substrates containing ITO (10 Ω/sq, Psiotec Ltd.) were cleaned by subsequent ultrasonic treatments in acetone, isopropanol and ethanol (15 min each) and finally dried with nitrogen. Then, the substrates were treated with plasma/O2 (10 sccm, 120 W, 60 s). The PEDOT:PSS (Clevios P VP AI4083, H. C. Starck GmbH) layer was spincoated (4000 rpm/60s) over the plasma treated ITO and then annealed at 120 ◦C for 3h, resulting in homogeneous layers of 30 nm. Concerning the active layer, all solutions contained the corresponding blue dye in a concentration of 10 mg/mL. In the case of iridium containing solutions, they were also prepared in a concentration of 10 mg/ mL of blue dye with different iridium ratio, in a proportion (w/w) of compound:Ir(MDQ)2acac:Ir(ppy)3 expressed as 100:x:y (x and y are detailed in Table 3). The active layers were deposited by spin-coating (1000 rpm/60 s) and dried under vacuum for 1 h. All spin-coating deposition processes were carried out under aerated conditions. Afterwards, the TPBi (20 nm), Ca (14 nm) and Al (100 nm, Kurt & Lesker) were deposited by thermal evaporation under high vacuum (1×10^{-7} mbar), using the shadow mask defining an active device area of 5 mm2. The devices were encapsulated with epoxy resin (Ossila E132), then covered by cover glass 20 × 20 mm (Deltalab, D102020) under N2 atmosphere, and subsequently cured in an UV oven Dymax 2000-PC for 60 s.

The thickness of the layers was determined with a Dektak XT, Veeco profilometer. The device optoelectronic characterization was performed in a Keithley 2604B SourceMeter and a photodiode (Thorlabs, SM1PD2A) governed by ir house software. The electroluminescence spectra were recorded with a spectrophotometer Ocean Optics USB2000+ and using SpectraSuite software.

3. RESULTS AND DISCUSSION

3.1. Synthesis and characterization

Considering the aforementioned building block, two new structural derivatives were designed and synthesized, namely 6,6′ -bis(phenylethynyl)- 9H,9′H-3,3′ -bicarbazole and 1,3,5-tris((9H-carbazol-3-yl) ethynyl)benzene. Each structure features two products with two different N-alkyl chain lengths, in order to evaluate their effect on the aggregation and disposition within the devices. The followed synthetic routes are depicted in Scheme 1. The synthetic precursors were obtained alkylating the commercially available 9H-carbazole and 3-iodo-9Hcarbazole [32] under standard conditions [29]. Compounds 1a-b were prepared by oxidative dimerization of the corresponding alkylated 9H-carbazole using $FeCl_3$ in anhydrous chloroform at room temperature [33]. Iodination in 6,6′ positions using KI and KIO_3 in acetic acid afforded the intermediates 2a-b [32]. Finally, the Sonogashira coupling reaction between 2a-b and phenylacetylene furnished the final compounds 3a-b [34]. Compounds 4a-b were also obtained through a Sonogashira coupling reaction, but in this case using the corresponding alkylated 3-iodo-9H-carbazole and 1,3,5-triethynylbenzene as starting materials. An alternative synthetic approach for 4a-b was also investigated, implying the attachment of the triple bond to the corresponding alkylated 3-iodo-9H-carbazole and the subsequent attachment of three 3-ethynyl-9H-carbazole units to 1,3,5-tribromobenzene through Sonogashira coupling reactions. This strategy, however, proved to be inadequate.

3.2. Photophysical properties

All compounds are soluble in common organic solvents. Photophysical properties of compounds 3a-b and 4a-b in solution and in the solid state are summarized in Table 1. The fluorescence measurements, performed in tetrahydrofuran solutions upon excitation at the maximum absorption wavelength, show a maximum at 416 nm for compounds 3ab and a double maximum at 369 and 380 nm for compounds 4a-b (Fig. 2). The structural disposition of the aromatic core affects significantly, since the bicarbazole derivatives emit at higher wavelengths than the triethynylbenzene-centered ones. Regarding the alkyl chain length, it does not influence the optical properties of neither of the two cores in solution but is decisive at modulating the emission in the solid state, highlighting its effect over the intermolecular arrangement. Whereas the difference between 4a and 4b concerning the emission spectra in the solid state is barely noticeable (4a, with the short ethyl chain, is 10 nm red-shifted with respect to 4b), it affects the emitted color between 3a and 3b. The hexylated derivative 3b, with a sharp band peaking at 428 nm, is the only one strictly showing deep-blue coordinates, while the ethylated analogue 3a, albeit having the maximum at the same wavelength, displays a broader band that results into emission within the blue-green region. The intermolecular arrangement and, consequently, the optical properties of the bicarbazole derivative 3 are therefore highly dependent on the alkyl chain nature. In order to further investigate this phenomenon, the single crystal structures of 3a and 3b were investigated by means of single crystal X-ray analysis (Fig. 3, Table S1 in the Supporting Information). Compound 3a crystallized in space group P-1 of the triclinic system. It must be mentioned that, despite the efforts invested in obtaining proper crystals of 3a, they could not provide enough reflexes to accurately resolve the structure. Nevertheless, the resulting data can be used to shed light on the influence of the intermolecular disposition on the emission in the solid state. The disposition of 3a suggests aggregation of the π-system of adjacent molecules, with π-π stacking distances up to 3.35 Å. The broadening of the emission band in the solid state is therefore likely to be caused by aggregation. Remarkably, the molecules contained into the unit cell have two different dispositions concerning the carbazole rings, namely cis and trans dispositions. Respecting compound 3b, it crystallized in space group P21/c of the monoclinic system. As expected from the sharp peak

with very low red-shift in the solid-state emission, the disposition of 3b within the unit cell does not show any appreciative π-π stacking interaction. In fact, the shortest intermolecular π-π distances found have values up to 4.83 Å. Contrarily, C–H···π interactions are predominant and determine the intermolecular packing motive. Regarding the intramolecular disposition, neither the phenyl nor the carbazole rings are coplanar with each other, with a deviation of planarity that disfavor aggregation. Quantitatively, compound 3b provides enhanced emission in the solid state [35–38], with quantum yield values of 0.11 and 0.21 in solution and in the solid state, respectively. On the other hand, compound 3a presents a slight decrease of the quantum yield, from 0.11 in solution to 0.07 in the solid state, commonly observed in molecules that present π-π stacking [39]. These results agree with the reported crystallographic data, pointing out the relevance of the alkyl chain length in this structure. In addition, the influence of the bicarbazole core on the photophysical properties of 3a-b has been analyzed by comparing them with those of their carbazole containing counterpart. The 3,6-bis(2-phenylethynyl)-9H-carbazole core, reported in the literature [29], shows aggregation caused quenching regardless of the N-alkyl chain length. It features quantum yield values around 0.27 and 0.11 in solution and in the solid state, respectively, with color coordinates far from the sought deep-blue emission in the solid state, pointing out the importance of the structural design of 3b. Regarding compounds 4a-b, they provide the highest quantum yield values among the synthesized dyes (0.82 and 0.80, respectively) in solution. However, the quantum yield in the solid state diminishes regardless of the alkyl chain, resulting in values of 0.08 and 0.07 for compounds 4a and 4b, respectively. The considerable decay of the quantum yield observed for the triethynylbenzene derivatives could be correlated to a higher planarity conferred by the rigidity of the triple bond spacers, making these compounds more prone to aggregation caused quenching.

3.3. Electrochemical properties

Electrochemical properties of compounds 3a-b and 4a-b were analyzed. Cyclic voltammetry measurements were carried out in dichloromethane, using TBAP as the supporting electrolyte. All compounds undergo an oxidation process, which is reversible for compounds 3a-b and irreversible for compounds 4a-b (Fig. S1 in the Supporting Information). No reduction processes were observed for any of the synthesized compounds. The electrochemical data and the resulting characteristics are collected in Table 1. Taking into account their ionization potential (IP) values, which were estimated from the oxidation onset potential values by cyclic voltammetry, and their optical gap energy values, obtained from the corresponding absorption spectra, all of them display characteristics typically found in reported p-type semiconductors [20,41–43]. It should be noticed that the IP values obtained for the bicarbazole derivatives are lower than those of the triethynylbenzene derivatives. On the other hand, the alkyl chain nature does not imply significant changes in the electrochemical properties.

3.4. Charge transport properties

The charge-transporting properties of the two molecular constructions have been examined. The measurements were performed by the time-of-flight (TOF) and xerographic time-of-flight (XTOF) techniques on solution-deposited layers. The obtained results, including the representative TOF and XTOF transients in the log-log scale and the electric field dependences of the charge drift mobility, are compiled in the Supporting Information (Table S2, Fig. S2). The transient curves in the linear scale show a dispersive behavior, so the transient times were determined in the log-log scale. Both structures exhibit holetransporting properties, with similar mobility values around 10^{-3} cm^2 V^{-1} s^{-1} at high electric fields up to 9 × 105 V cm^{-1}, but neither of them displayed electron-transporting properties. Hence, both molecular constructions behave as p-type organic semiconductors.

3.5. Organic Light-Emitting Diodes

In view of the resulting photophysical and electrochemical features, i.e. p-type semiconducting properties and strong emission within the blue region of the visible spectrum, compounds 3–4 are good candidates to be explored in the OLED technology. Also, they show high thermal stability with decomposition temperatures (Td) higher than 400 ◦C (Table S3, Supporting Information). Henceforth, compounds 3–4 have been tested as emissive layer components alone in non-doped OLEDs and in combination with iridium complexes in WOLEDs as a proof of concept. A simple and compatible with solution processing OLED construction has been chosen, which consists on ITO/PEDOT:PSS (25 nm)/compound:Ir(MDQ)2acac:Ir(ppy)3 (33–80 nm)/TPBi (20 nm)/Ca (14 nm)/Al (100 nm), where the emissive layer composition and thickness depend on the type of device. Fig. 4 depicts a schematic representation of the energy levels of all compounds involved in the construction.

In order to evaluate the effectiveness of the synthesized compounds as emitters, we prepared blue-emitting OLEDs as a first approach to study their performance on final devices. Concerning the solutionprocessed deposition of the emissive layer, different solvents were considered. All compounds were tested using tetrahydrofuran (THF) and chlorobenzene (CB). As observed in Table 2, devices fabricated from THF solutions underperformed in front of the ones fabricated using CB, in terms of both luminance and current efficiency. The resulting turn-on voltage and the thickness of the films were also considerably higher for those prepared from THF. The use of cyclohexanone (CH) was discarded because of the poor performance of the corresponding device (Device 3). Hence, CB was selected for posterior studies. All bicarbazole-based (3ab) and triethynylbenzene-based (4a-b) compounds display luminance values from 101 to 102 cd m 2. Remarkably, the maximum luminance values were achieved with 3a and 4b, which are the ethylated derivative for the former structure and the 2-ethylhexylated derivative for the latter, respectively. In terms of current efficiency, the better results are obtained in devices based on compounds 4a-b.

Going one step further, we evaluated the synthesized compounds in the preparation of WOLEDs. For that, we combined each blue-emitting carbazole derivative with the commercially available Ir(MDQ)2acac and Ir(ppy)3 complexes using chlorobenzene as solvent. Both compounds featuring the ethyl chain, namely 3a and 4a, proved to be unappropriated for this study. Specifically, 3a led to a slight deviance from the targeted white light due to its blue-green emission in the solid state, while 4a furnished devices with heterogeneous layers derived from the solution processing that prevented a proper measurement. Regarding 4b, the first attempts of obtaining white light did not imply an improvement of luminance and efficiency with respect to the corresponding blue OLED (Table 2, Device 9), so it was not considered for further experiments (optoelectronic properties of iridium-containing devices based on 3a and 4b are summarized in the Supporting Information). On the contrary, devices composed by compound 3b revealed it as the best candidate to perform as both host and blue emitter in WOLEDs. The phosphorescence spectra of compounds 3b and 4b (Fig. S4, Supporting Information) indicate that compound 3b possesses a higher triplet energy than 4b, with values of 2.66 and 2.56 eV, respectively, which is associated to a more effective host-to-guest energy transfer [44,45]. The optoelectronic properties of a representative set of devices fabricated from 3b with different proportions of the commercial iridium complexes are shown in Table 3. The first tests (Devices 10–11) were performed in combination with a single iridium emitter as references. Notably, the combination with the green emitting complex Ir (ppy)3, which features a triplet energy level closer to that of the blue emitter, provides better performance than the red one Ir(MDQ)2acac, in terms of both luminance and efficiency. In fact, the former outdoes with a maximum current efficiency value of 1.73 cd A^{-1}, in front of 0.39 cd A^{-1} of the latter, pointing out the relevance of balanced triplet energy levels. The overlap between the absorption and emission spectra of the synthesized compounds and the reported for both iridium complexes [47,48] is also indicative of the feasibility of host–to-guest energy transfer.

Fig. 5 depicts the optoelectronic properties of devices based on compound 3b containing a single iridium complex (Devices 10 and 11) and those with an equal proportion of both iridium complexes (Devices 12–15). In terms of color, all devices combining both iridium complexes within the emissive layer closely adjust to the Planckian locus (represented in Fig. 5b). Specifically, a ratio of 3b:Ir(MDQ)2acac:Ir(ppy)3 of 100:0.12:0.12 (Device 12) provides pure white coordinates at 6 V, i.e. (0.33, 0.33) (Fig. 6a), and a color temperature of 5617 K, with balanced emission of all three components. It should be highlighted that the equality of emission intensity between Ir(MDQ)2acac and Ir(ppy)3 is lost at higher proportions of iridium complexes than the aforementioned (Devices 13–15). In fact, the red emission corresponding to Ir (MDQ)2acac surpasses the green one from Ir(ppy)3, leading to color coordinates closer to the Planckian locus. Consequently, the produced white light can be finely tuned with small variations of the emissive layer composition, tending to lower color temperature values at higher percentages of iridium complexes, i.e. warmer white in terms of illumination.

It is also significant the effect of the applied voltage as modulator of the emitted white color. Fig. 6 represents the electroluminescent properties of devices 12 and 14 to exemplify its effect. Considering the studied devices, the host 3b contribution to the blue emission is generally maximized at lower voltages, whereas more transference to the red Ir(MDQ)2acac is observed at higher voltages. This points to a voltage-dependent energy transfer towards the red-emitting Ir (MDQ)2acac. Then, the color temperature of a device can be adapted working with the voltage as a modulating factor.

4. CONCLUSIONS

Two new carbazole-based structures featuring two different N-alkyl chain lengths have been developed. All the synthesized compounds display interesting optoelectronic properties that are influenced by their molecular construction. Remarkably, the presence of the bicarbazole core and the length of the N-alkyl chains are crucial for the chromophores based on the 3-(phenylethynyl)-9H-carbazole moiety, determining the intermolecular arrangement and, therefore, their optical properties in the solid state. Specifically, the N-hexylated derivative 3b not only displays deep-blue emission, but also is an appropriate host for iridium complexes to build solution-processed WOLEDs. In fact, the combination of 3b with a 0.12% of each iridium complex provides pure white coordinates at 6 V. The emission of the resulting devices, which depends on the ratio of the iridium complexes and the applied voltage, covers a vast range of correlated color temperatures.

CRediT authorship contribution statement

Roger Bujaldón: Investigation, Writing - original draft. Nikola Peřinka: Investigation. Marta Reig: Investigation. Alba Cuadrado: Investigation. Clara Fabregat: Investigation. Mercè Font-Bardía: Formal analysis. Eugenia Martínez-Ferrero: Conceptualization. Dolores Velasco: Conceptualization, Supervision.

Declaration of competing interest

The authors declare that they have no known competing financial interests or personal relationships that could have appeared to influence the work reported in this paper.

ACKNOWLEDGEMENTS

Financial support from the Ministerio de Economía y Competitividad (FUNMAT-PGC2018-095477-B-I00) and Eurecat (IMPLLUM) is gratefully acknowledged. The authors acknowledge Prof. J. V. Grazulevicius and Prof. V. Jankauskas for their assistance in the TOF-XTOF measurements. R. B. is grateful for the grant FI AGAUR from Generalitat de Catalunya, Spain

References

[1] Q. Wei, N. Fei, A. Islam, T. Lei, L. Hong, R. Peng, X. Fan, L. Chen, P. Gao, Z. Ge, Small-molecule emitters with high quantum efficiency: mechanisms, structures, and applications in OLED Devices, Adv. Optical Mater. 6 (2018) 1800512.

[2] A. Salehi, X. Fu, D.-H. Shin, F. So, Recent advances in OLED optical design, Adv. Funct. Mater. 29 (2019) 1808803.

[3] J.-H. Jou, S. Sahoo, D.K. Dubey, R.A.K. Yadav, S.S. Swayamprabha, S.D. Chavhan, Molecule-based monochromatic and polychromatic OLEDs with wet-process feasibility, J. Mater. Chem. C 6 (2018) 11492–11518.

[4] F. Guo, A. Karl, Q.-F. Xue, K.C. Tam, K. Forberich, C.J. Brabec, The fabrication of color-tunable organic light-emitting diode displays via solution processing, Light Sci. Appl. 6 (2017), e17094.

[5] M. Cai, T. Xiao, E. Hellerich, Y. Chen, R. Shinar, J. Shinar, High-efficiency solutionprocessed small molecule electrophosphorescent organic light-emitting diodes, Adv. Mater. 23 (2011) 3590–3596.

[6] C. Sartorio, V. Fig`a, P. Salice, D. Gragnato, S. Cataldo, M. Scopelliti, R. Improta, E. Menna, B. Pignataro, Thiophene pyrenyl derivatives for the supramolecular processability of single-walled carbon nanotubes in thin film heterojunction, Synth. Met. 229 (2017) 7–15.

[7] D. Liu, W. Tian, Y. Feng, X. Zhang, X. Ban, W. Jiang, Y. Sun, Achieving 20% external quantum efficiency for fully solution-processed organic light-emitting diodes based on thermally activated delayed fluorescence dendrimers with flexible chains, ACS Appl. Mater. Interfaces 11 (2019) 16737–16748.

[8] X. Zheng, Y. Liu, Y. Zhu, F. Ma, C. Feng, Y. Yu, H. Hu, F. Li, Efficient inkjet-printed blue OLED with boosted charge transport using host doping for application in pixelated display, Opt. Mater. 101 (2020) 109755.

[9] L. Derue, S. Olivier, D. Tondelier, T. Maindron, B. Geffroy, E. Ishow, All-solutionprocessed organic light-emitting diodes based on photostable photo-cross-linkable fluorescent small molecules, ACS Appl. Mater. Interfaces 82 (2016) 16207–16217.

[10] N. Aizawa, Y.-J. Pu, M. Watanabe, T. Chiba, K. Ideta, N. Toyota, M. Igarashi, Y. Suzuri, H. Sasabe, J. Kido, Solution-processed multilayer small-molecule lightemitting devices with high-efficiency white-light emission, Nat. Commun. 5 (2014) 5756.

[11] B. Liu, X.-L. Li, H. Tao, J. Zou, M. Xu, L. Wang, J. Peng, Y. Cao, Manipulation of exciton distribution for high-performance fluorescent/phosphorescent hybrid white organic light-emitting diodes, J. Mater. Chem. C 5 (2017) 7668–7683.

[12] H. Dong, H. Jiang, J. Wang, Y. Guan, J. Hua, X. Gao, B. Bo, J. Wang, Highefficiency and color-stable warm white organic light-emitting diodes utilizing energy transfer from interface exciplex, Org. Electron. 62 (2018) 524–529.

[13] H. Peng, Z. Wei, L. Wu, X. Li, Efficient non-doped blue fluorescent OLEDs based on bipolar phenanthroimidazole-triphenylamine derivatives, Opt. Mater. 101 (2020) 109726.

[14] B. Wex, B.R. Kaafarani, Perspective on carbazole-based organic compounds as emitters and hosts in TADF applications, J. Mater. Chem. C 5 (2017) 8622–8653.

[15] M.M.L. Kadam, D. Patil, N. Sekar, Fluorescent carbazole based pyridone dyes – synthesis, solvatochromism, linear and nonlinear optical properties, Opt. Mater. 85 (2018) 308–318.

[16] T. Zhang, J. Ye, A. Luo, D. Liu, Efficient deep blue emitter based on carbazolepyrene hybrid for non-doped electroluminescent device, Opt. Mater. 100 (2020) 109632.

[17] C. Bian, Q. Wang, Q. Ran, X.-Y. Liu, J. Fan, L.S. Liao, New carbazole-based bipolar hosts for efficient blue phosphorescent organic light-emitting diodes, Org. Electron. 52 (2018) 138–145.

[18] J. Ji, P. Li, Q. Tian, W. Feng, C. Wu, Three new carbazole derivatives with high thermal stability as host for efficient green phosphorescent organic-light emitting diodes, Dyes Pigments 171 (2019) 107670.
[19] M. Reig, J. Puigdollers, D. Velasco, Solid-state organization of n-type carbazolebased semiconductors for organic thin-film transistors, Phys. Chem. Chem. Phys. 20 (2018) 1142–1149.
[20] M. Reig, G. Bagdziunas, A. Ramanavicius, J. Puigdollers, D. Velasco, Interface engineering and solid-state organization for triindole-based p-type organic thinfilm transistors, Phys. Chem. Chem. Phys. 20 (2018) 17889–17898.
[21] S.-L. Lin, L.-H. Chan, R.-H. Lee, M.-Y. Yen, W.-J. Kuo, C.-T. Chen, R.-J. Jeng, Highly efficient carbazole-π-dimesitylborane bipolar fluorophores for nondoped blue organic light-emitting diodes, Adv. Mater. 20 (2008) 3947–3952.
[22] M. Yu, S. Wang, S. Shao, J. Ding, L. Wang, X. Jing, F. Wang, Starburst 4,4',4''-tris (carbazol-9-yl)-triphenylamine-based deep-blue fluorescent emitters with tunable oligophenyl length for solution-processed undoped organic light emitting diodes, J. Mater. Chem. C 3 (2015) 861–869.
[23] J.-H. Jou, J.-L. Li, S. Sahoo, D.K. Dubey, R.A.K. Yadav, V. Joseph, K.R.J. Thomas, C.-W. Wang, J. Jayakumar, C.-H. Cheng, Enabling a 6.5% external quantum efficiency deep-blue organic light-emitting diode with a solution-processable carbazole-based emitter, J. Phys. Chem. C 122 (2018) 24295–24303.
[24] V. Joseph, K.R.J. Thomas, S. Sahoo, M. Singh, J.-H. Jou, Simple carbazole based deep-blue emitters: the effect of spacer, linkage and end-capping cyano group on the photophysical and electroluminescent properties, Dyes Pigments 151 (2018) 310–320.
[25] S. Kato, H. Noguchi, A. Kobayashi, T. Yoshihara, S. Tobita, Y. Nakamura, Bicarbazoles: systematic structure-property investigations on a series of conjugated carbazole dimers, J. Org. Chem. 77 (2012) 9120–9133.
[26] B. Zhao, X. Jia, J. Liu, X. Ma, H. Zhang, X. Wang, T. Wang, Synthesis and characterization of novel 1,4-bis(carbazolyl)benzene derivatives with blue-violet two-photon-excited fluorescence, Ind. Eng. Chem. Res. 55 (2016) 1801–1807.
[27] A. Slodek, M. Filapek, E. Schab-Balcerzak, M. Grucela, S. Kotowicz, H. Janeczek, K. Smolarek, S. Mackowski, J.G. Malecki, A. Jedrzejowska, G. Szafraniec-Gorol, A. Chrobok, B. Marcol, S. Krompiec, M. Matussek, Highly luminescence anthracene derivatives as promising materials for OLED applications, Eur. J. Org Chem. 23 (2016) 4020–4031.
[28] M. Reig, G. Bubniene, W. Cambarau, V. Jankauskas, V. Getautis, E. Palomares, E. Martínez-Ferrero, D. Velasco, New solution-processable carbazole derivatives as deep blue emitters for organic light-emitting diodes, RSC Adv. 6 (2016) 9247–9253.
[29] M. Reig, C. Gozalvez, R. Bujaldon, G. Bagdziunas, K. Ivaniuk, N. Kostiv, D. Volyniuk, J.V. Grazulevicius, D. Velasco, Easy accessible blue luminescent carbazole-based materials for organic light-emitting diodes, Dyes Pigments 137 (2017) 24–35.
[30] J.N. Demas, G.A. Crosby, Measurement of photoluminescence quantum yields, Rev. J. Phys. Chem. 75 (1971) 991–1024.
[31] C.M. Cardona, W. Li, A.E. Kaifer, D. Stockdale, G.C. Bazan, Electrochemical considerations for determining absolute frontier orbital energy levels of conjugated polymers for solar cell applications, Adv. Mater. 23 (2011) 2367–2371.
[32] S.H. Tucker, Iodination in the carbazole series, J. Chem. Soc. 129 (1926) 546–553.
[33] H. Wang, G. Chen, X. Xu, H. Chen, S. Ji, The synthesis and optical properties of benzothiazole-based derivatives with various p-electron donors as novel bipolar fluorescent compounds, Dyes Pigments 86 (2010) 238–248.
[34] R. Chinchilla, C. N´ajera, The Sonogashira reaction: a booming methodology in synthetic organic chemistry, Chem. Rev. 107 (2007) 874–922.

[35] Y. Kubota, K. Kasatani, H. Takai, K. Funabiki, M. Matsui, Strategy to enhance solidstate fluorescence and aggregation-induced emission enhancement effect in pyrimidine boron complexes, Dalton Trans. 44 (2015) 3326–3341.
[36] L. Kong, Z. Huang, Q.-Y. Chen, H.-C. Zhu, H. Wang, X.-Y. Xu, J.-X. Yang, Aggregation-induced enhanced emission of a carbazole derivative with asymmetric group, Opt. Mater. 82 (2018) 154–159.
[37] M. Matsui, K. Ooiwa, A. Okada, Y. Kubota, K. Funabiki, H. Sato, Solid-state fluorescence of pyridinium styryl dyes, Dyes Pigments 99 (2013) 916–923.
[38] S.-Y. Park, M. Ebihara, Y. Kubota, K. Funabiki, M. Matsui, The relationship between solid-state fluorescence intensity and molecular packing of coumarindyes, Dyes Pigments 82 (2009) 258–267.
[39] J.N. Moorthy, P. Natarajan, P. Venkatakrishnan, D.-F. Huang, T.J. Chow, Steric inhibition of π-stacking: 1,3,6,8-tetraarylpyrenes as efficient blue emitters in organic light emitting diodes (OLEDs), Org. Lett. 9 (2007) 5215–5218.
[40] Y.-M. Xie, L.-S. Cui, Y. Liu, F.-S. Zu, Q. Li, Z.-Q. Jiang, L.-S. Liao, Efficient blue/white phosphorescent organic light-emitting diodes based on a silicon-based host material via a direct carbon–nitrogen bond, J. Mater. Chem. C 3 (2015) 5347–5353.
[41] H. Bronstein, C.B. Nielsen, B.C. Schroeder, I. McCulloch, The role of chemical design in the performance of organic semiconductors, Nat. Rev. 4 (2020) 66–77.
[42] K. Takimiya, T. Yamamoto, H. Ebata, T. Izawa, Design strategy for air-stable organic semiconductors applicable to high-performance field-effect transistors, Sci. Technol. Adv. Mater. 8 (2007) 273–276.
[43] A. Cuadrado, J. Cuesta, J. Puigdollers, D. Velasco, Air stable organic semiconductors based on diindolo[3,2-a:3',2'-c]carbazole, Org. Electron. 62 (2018) 35–42.
[44] L. Zhu, Z. Wu, J. Chen, D. Ma, Reduced efficiency roll-off in all-phosphorescent white organic light-emitting diodes with an external quantum efficiency of over 20%, J. Mater. Chem. C 3 (2015) 3304–3310.
[45] Y. Li, L. Zhou, R. Cui, Y. Jiang, X. Zhao, W. Liu, Q. Zhu, Y. Cui, H. Zhang, High performance red organic electroluminescent devices based on a trivalent iridium complex with stepwise energy levels, RSC Adv. 6 (2016) 71282–71286.
[46] C.S. McCamy, Correlated color temperature as an explicit function of chromaticity coordinates, Color Res. Appl. 17 (1992) 142–144.
[47] S.M. King, H.A. Al-Attar, R.J. Evans, A. Congreve, A. Beeby, A.P. Monkman, The use of substituted iridium complexes in doped polymer electrophosphorescent devices: the influence of triplet transfer and other factors on enhancing device performance, Adv. Funct. Mater. 16 (2006) 1043–1050.
[48] Y.-L. Chang, Y. Song, Z. Wang, M.G. Helander, J. Qiu, L. Chai, Z. Liu, G.D. Scholes, Z. Lu, Highly efficient warm white organic light-emitting diodes by triplet exciton conversion, Adv. Funct. Mater. 23 (2013) 705–712.

Table 1. Optical and electrochemical properties for compounds 3a-b and 4a-b in solution and in the solid state.

	λ_{abs}[a] (nm)	λ_{em}[a] (nm)	Φ_f[a]	λ_{em}[b] (nm)	Φ_f[b]	CIE[b]	E_{gap}[c] (eV)	$^{ox}E_{onset}$[d] (V)	IP[e] (eV)	EA[f] (eV)
3a	313, 337	416	0.11	428	0.07	(0.20, 0.20)	3.35	0.41	5.80	2.45
3b	313, 337	416	0.11	428	0.21	(0.17, 0.10)	3.35	0.41	5.80	2.45
4a	304, 332	369, 380	0.82	410	0.08	(0.17, 0.11)	3.34	0.57	5.96	2.62
4b	304, 332	369, 380	0.80	400	0.07	(0.17, 0.12)	3.34	0.61	6.00	2.66

[a] Measured in THF at 10 µM. Quantum yield measurements were performed after excitation at 300 nm using POPOP (1,4-bis(5-phenyl-2-oxazolyl)benzene) as standard.

[b] Measured in thin films over quartz substrates.

[c] Optical gap energy.

[d] Onset oxidation potential determined from cyclic voltammetry in CH_2Cl_2 (1 mM).

[e] Ionization potential estimated as IP = $^{ox}E_{onset}$ + 5.39.

[f] Electron affinity estimated as EA = IP - E_{gap}.

Table 2. Characteristics obtained for OLED devices fabricated from compounds 3a-b and 4a-b.

	Dev.	Solvent[a]	d (nm)[b]	V_{on} (V)[c]	L_{max} (cd m^{-2})[d]	CE (cd A^{-1})[e]
3a	1	THF	51 ± 2	5.2	41	0.05
	2	CB	33 ± 2	3.8	119	0.08
3b	3	CH	33 ± 2	5.7	9	0.04
	4	THF	49 ± 8	7.8	18	0.02
	5	CB	37 ± 4	5.0	43	0.05
4a	6	THF	71 ± 6	6.4	19	0.04
	7	CB	43 ± 4	4.9	38	0.09
4b	8	THF	79 ± 2	8.2	44	0.12
	9	CB	44 ± 4	4.5	101	0.33

[a] Solvent used for preparing the spin-casted layer, namely tetrahydrofuran (THF), chlorobenzene (CB) and cyclohexanone (CH).

[b] Average thickness of the emitting layer.

[c] Turn-on voltage defined as the voltage corresponding to a luminance of 1 cd m^{-2}.

[d] Maximum luminance.

[e] Maximum current efficiency.

Table 3. Characteristics of OLEDs containing compound 3b as the blue emitter along with different proportions of $Ir(MDQ)_2acac$ and $Ir(ppy)_3$.

Dev.	3b	$Ir(MDQ)_2acac$[a]	$Ir(ppy)_3$[a]	V_t (V)[b]	L_{max} (cd m^{-2})[c]	CE (cd A^{-1})[d]	CIE[e]	T (K)[f]
10	100	1.00	–	4.8	142	0.39	(0.52, 0.40)	1974
11	100	–	1.00	3.7	186	1.73	(0.28, 0.57)	–
12	100	0.12	0.12	4.2	58	0.03	(0.35, 0.33)	4852
13	100	0.25	0.25	3.8	66	0.22	(0.42, 0.40)	3276
14	100	0.50	0.50	3.4	204	0.66	(0.45, 0.44)	3012
15	100	1.00	1.00	3.7	288	1.57	(0.47, 0.45)	2821

[a] Proportion (w/w) of iridium complexes in front of 3b (Ratio of 3b:$Ir(MDQ)_2acac$:$Ir(ppy)_3$).

[b] Turn-on voltage defined as the voltage corresponding to a luminance of 1 cd m^{-2}.

[c] Maximum luminance.

[d] Maximum current efficiency.

[e] CIE coordinates calculated from the corresponding electroluminescence spectrum at 10 V for devices 10–11 and at 8 V for devices 12–15.

[f] Correlated color temperature calculated from the obtained CIE coordinates using the McCamy's approximation [46].

Figure Captions

Figure. 1. Schematic multilayer structure of a device and the emissive layer composition: the herein studied blue-emitting fluorophores, namely 6,6' -bis(phenylethynyl)-9H,9'H-3,3' -bicarbazole (left) and 1,3,5-tris((9H-carbazol-3-yl)ethynyl)benzene (right), and the iridium complexes $Ir(ppy)_3$ and $Ir(MDQ)_2acac$, displayinggreen and red emission, respectively. The 3-(phenylethynyl)-9H-carbazole scaffold is highlighted in blue in each structure. (For interpretation of the references to color in this figure legend, the reader is referred to the Web version of this article.)

Scheme 1. Synthetic routes towards the final products 3a-b and 4a-b. Reagents and conditions: (i) NaH in DMF, alkyl bromide, RT. (ii) $FeCl_3$ in $CHCl_3$, RT. (iii) KI, KIO_3 in acetic acid, reflux. (iv) $Pd(PPh_3)_2Cl_2$, CuI, triethylamine in THF, RT.

Figure. 2. Absorption (dashed) and emission (solid) spectra in THF (10^{-5} M) of a) compounds 3a-b and b) compounds 4a-b, excited at $\lambda_{ex} = \lambda_{abs,max}$ (see Table 1).Emission spectra in the solid state of compounds c) 3a-b and d) 4a-b, excited at 320 and 330 nm, respectively.

Figure. 3. Single crystal structures of compounds a) 3a and b) 3b. The amplified regions of the X-ray structures show a representative set of π-π distances for 3a and the dihedral angles for 3b from a different point of view, respectively. Hydrogen atoms have been omitted for clarity.

Figure. 4. Energetic scheme of the different components integrated on the OLED structure used in this study, including compounds 3a-b and 4a-b, $Ir(ppy)_3$ [10] and Ir $(MDQ)_2acac$ [40].

Figure. 5. Electroluminescence spectra (a), CIE coordinates (b), luminance (c) and current efficiency (d) of devices featuring compound 3b along with $Ir(MDQ)_2acac$ (Device 10), $Ir(ppy)_3$ (Device 11) and different 1:1 iridium complex ratios (Devices 12–15).

Figure. 6. Electroluminescence spectra and the corresponding CIE coordinates at different applied voltages (the lower represented in black and the higher in pale grey) of: a) Device 12 (100:0.12:0.12) and b) Device 14 (100:0.50:0.50). The corresponding data is compiled in Table S5 in the Supporting Information.

Figure 1.

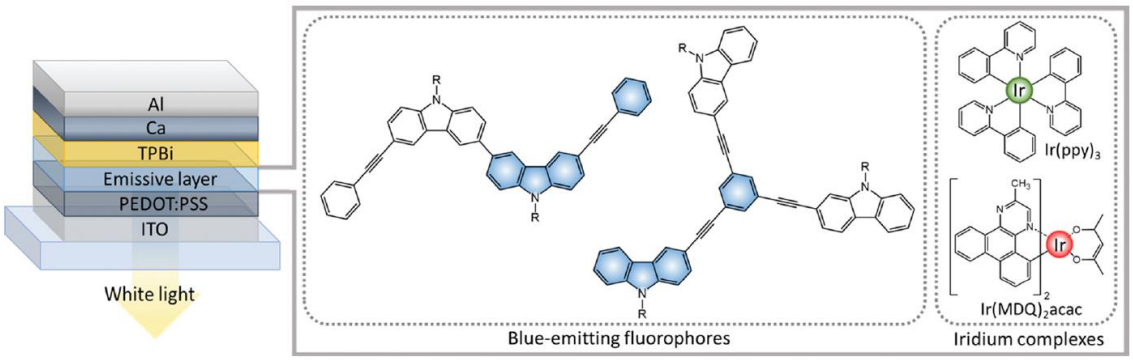
Al
Ca
TPBi
Emissive layer
PEDOT:PSS
ITO
White light
Blue-emitting fluorophores
Ir(ppy)3
Ir(MDQ)2acac
Iridium complexes

Scheme 1.

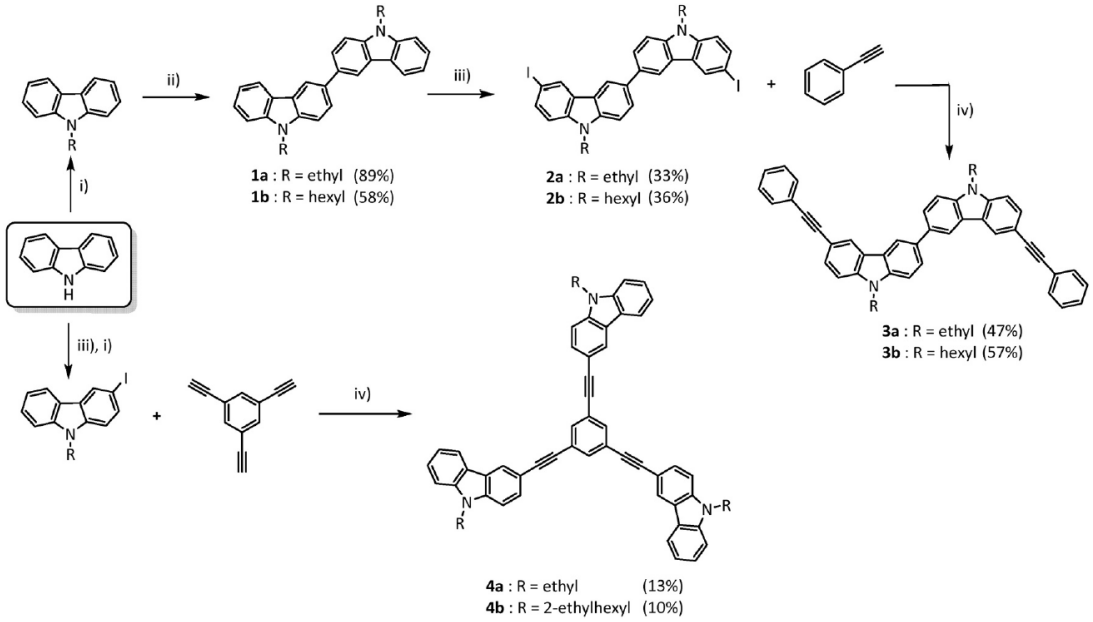
ii)
iii)
i)
iv)
iii), i)
iv)
1a : R = ethyl (89%)
1b : R = hexyl (58%)
2a : R = ethyl (33%)
2b : R = hexyl (36%)
3a : R = ethyl (47%)
3b : R = hexyl (57%)
4a : R = ethyl (13%)
4b : R = 2-ethylhexyl (10%)

Figure 2.

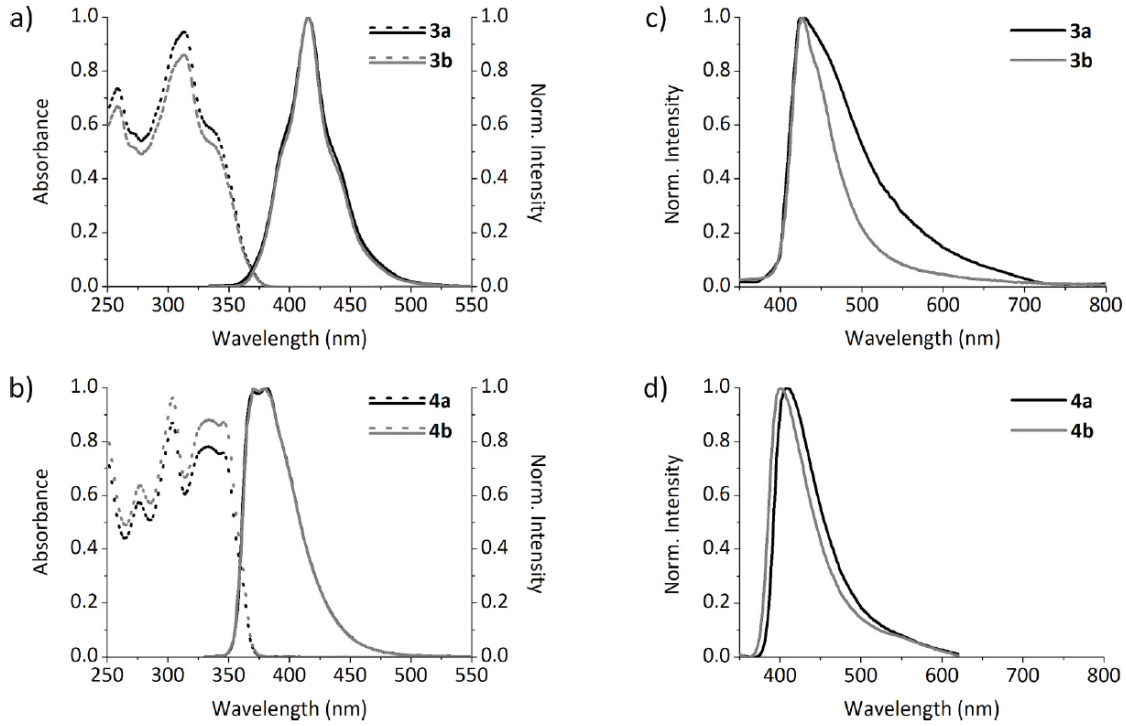

Figure 3

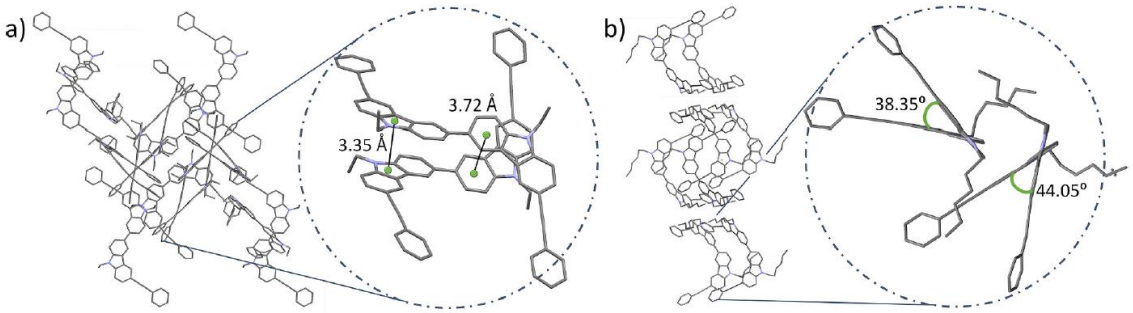

Figure 4

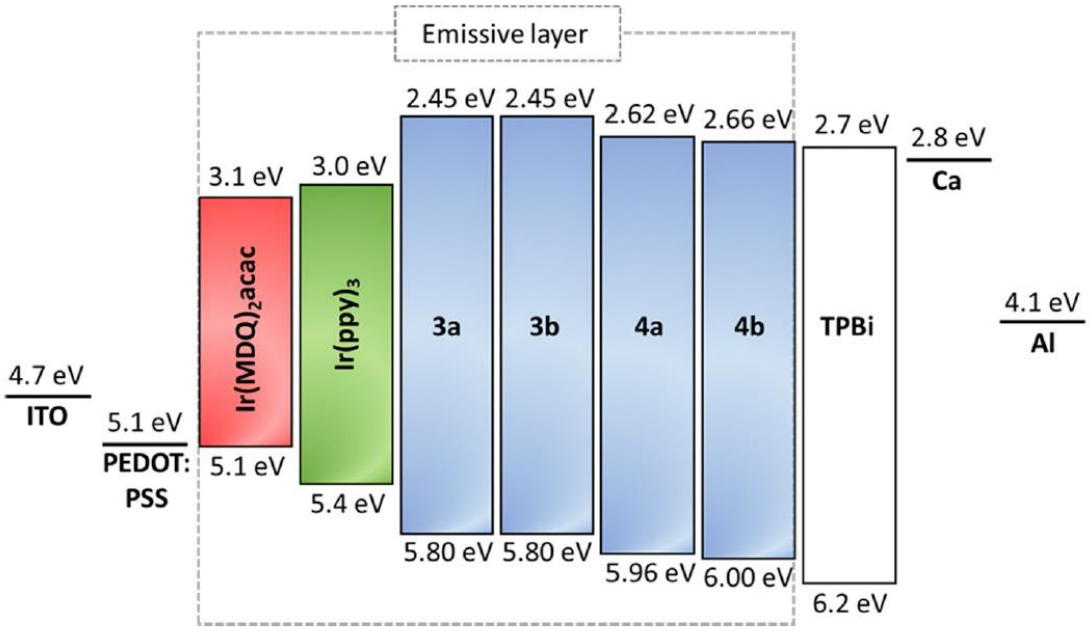
Emissive layer
4.7 eV
ITO
5.1 eV
PEDOT:
PSS
3.1 eV
Ir(MDQ)2acac
5.1 eV
3.0 eV
Ir(ppy)3
5.4 eV
2.45 eV
3a
5.80 eV
2.45 eV
3b
5.80 eV
2.62 eV
4a
5.96 eV
2.66 eV
4b
6.00 eV
2.7 eV
TPBi
6.2 eV
2.8 eV
Ca
4.1 eV
Al

Figure 5

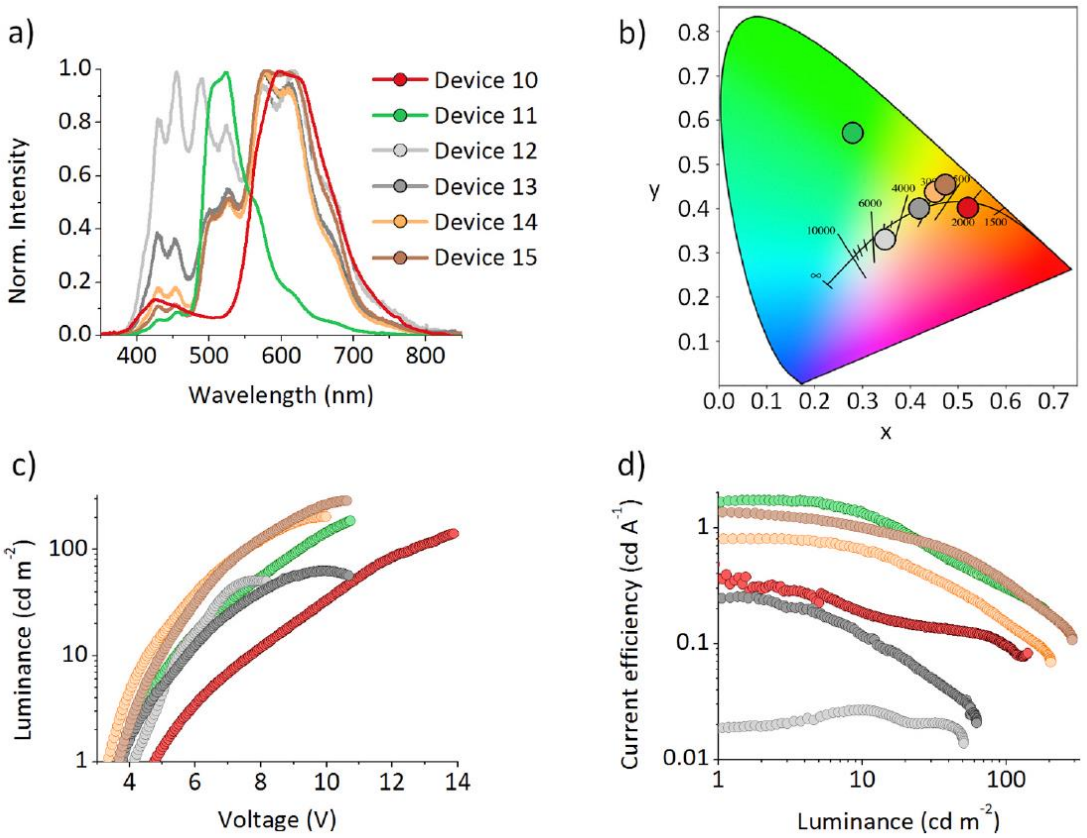
a)
Norm. Intensity
Wavelength (nm)
Device 10
Device 11
Device 12
Device 13
Device 14
Device 15
b)
y
x
c)
Luminance (cd m-2)
Voltage (V)
d)
Current efficiency (cd A-1)
Luminance (cd m-2)

Figure 6

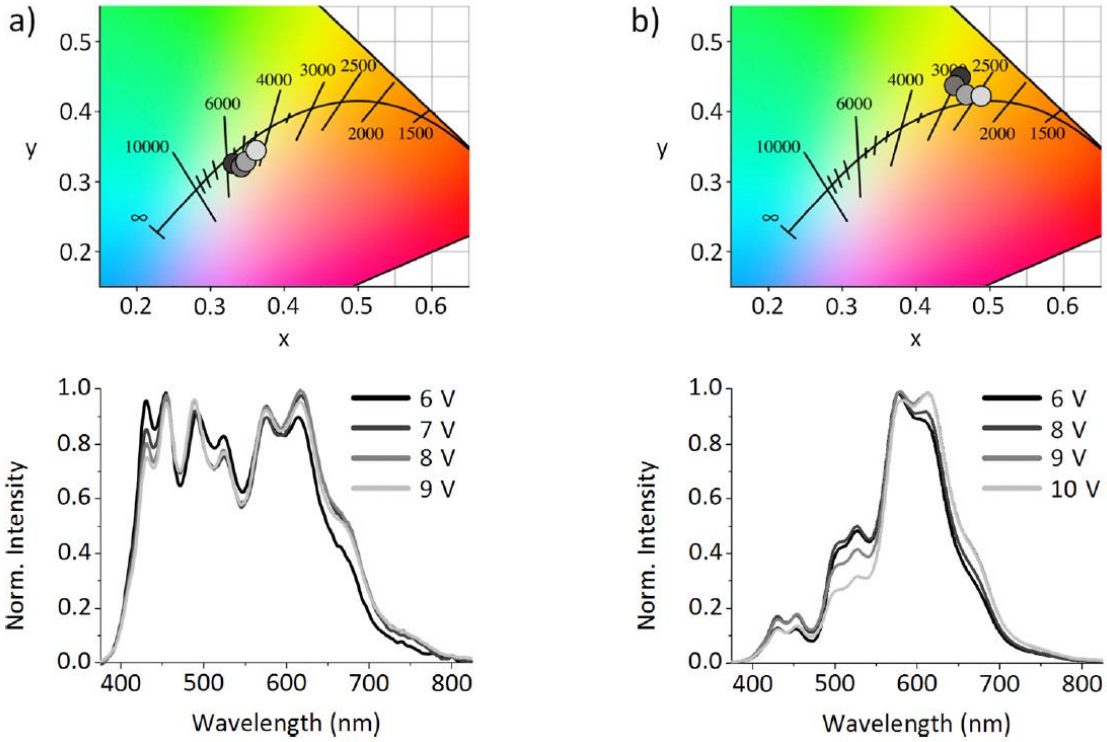
a)
b)
x
y
10000
6000
4000
3000
2500
2000
1500
∞
Norm. Intensity
Wavelength (nm)
6 V
7 V
8 V
9 V
10 V